Microelectronic Engineering 88 (2011) 3054–3061

Contents lists available at ScienceDirect

Microelectronic Engineering

journal homepage: www.elsevier.com/locate/mee

Experiment-based estimation of point spread function in electron-beam lithography: Forward-scattering part

Q. Dai [a], S.-Y. Lee [a,*], S.-H. Lee [b], B.-G. Kim [b], H.-K. Cho [b]

[a] Department of Electrical and Computer Engineering, Auburn University, Auburn, AL 36849, USA
[b] Samsung Electronics, Photomask Division, 16 Banwol-Dong, Hwasung, Kyunggi-Do, Republic of Korea

ARTICLE INFO

Article history:
Received 25 January 2011
Received in revised form 29 April 2011
Accepted 16 May 2011
Available online 23 May 2011

Keywords:
Convolution
Exposure
Line response function
Line spread function
Point spread function
Lateral development
Vertical development

ABSTRACT

The point spread function (*PSF*) plays an important role in electron beam (e-beam) lithography, e.g., estimation of resist profile, proximity effect correction, etc. One of the essential tasks is how to estimate the *PSF* with accuracy and efficiency. Conventional approaches include estimation of *PSF*'s based on certain functions or through a Monte Carlo simulation. A new approach to estimating *PSF*'s based on experimental data is proposed to provide an alternative to the conventional approaches. It utilizes the relationship between a *PSF* and a line spread function (*LSF*), and that between a *LSF* and the remaining resist profile. Since effects of all phenomena and processes involved in the exposure step are reflected in experimental results, the proposed approach has a good potential to generate realistic *PSF*'s for any substrates and e-beam tools as long as experiments can be carried out. In this paper, the implementation of the new approach for estimation of the forward scattering part of *PSF* is described along with the simulation and experiment results.

1. Introduction

The electron-beam (e-beam) lithographic process consists of exposing resist by e-beam and subsequently developing the resist for pattern transfer. For applications such as the proximity effect correction [1–6] and the estimation of remaining resist profiles [7–10], both steps are often simulated. The exposure (energy deposited in the resist) distribution essential in such applications is computed by the convolution between a circuit pattern (dose distribution) and a *point spread function* (*PSF*) which is radially symmetric and shows how the electron energy is distributed throughout the resist when a single point is exposed. Therefore, high accuracy of a *PSF* is crucial in the above-mentioned applications.

The *PSF* estimation schemes developed previously may be classified into two groups: Gaussian function fitting and Monte Carlo simulation. Chang used a double-Gaussian function to fit *PSF*'s [11], where one Gaussian function models the deposited energy due to the forward-scattering of electrons and the other Gaussian function that due to the backscattering of electrons. The parameter α in the model represents the forward-scattering range, the parameter β the backscattering range, and the parameter η the ratio of the backscattered energy level to the forward-scattered energy level. One problem of this double-Gaussian model is its inability to model the transition between the forward-scattering and backscattering regions. To enhance the accuracy of the model, more complicated forms of functions were proposed, such as the triple-Gaussian function, the quadruple-Gaussian function, and the double Gaussian function plus an exponential term [12–15]. A drawback of the curve fitting approaches is the difficulty in accurately determining the parameters. Based on the model of a double-Gaussian function plus an exponential term, Fastenau utilized the confocal scanning laser microscope to determine the parameters in an accurate way [16], however, the lateral development of resist was not considered. Instead of using the energy merit function to minimize the sum of energy deviations, Fretwell adopted a LOG merit function to determine the parameters of a normalized triple-Gaussian function by fitting to Monte Carlo data, which was well approximated in the transition region [17]. However, the LOG merit function was later reported to work well only for certain substrates such as gold [14]. Rooks proposed an experiment-based method for determining the optimal value of the parameter α for a double-Gaussian model of *PSF* [18].

The Monte Carlo simulation is another widely-used approach to deriving *PSF*'s. It traces individual electrons following the paths stochastically determined based on the phenomena and effects theoretically modeled. The accuracy of the *PSF*'s generated by such a simulation depends on the theoretical model employed and the number of electrons traced. As long as the number of electrons is

* Corresponding author. Fax: +1 334 844 1809.
E-mail address: leesooy@eng.auburn.edu (S.-Y. Lee).

0167-9317/$ - see front matter © 2011 Elsevier B.V. All rights reserved.
doi:10.1016/j.mee.2011.05.019

sufficiently large and all or most of the major phenomena and effects are modeled, the *PSF*'s are considered to be accurate. The programs based on the Monte Carlo simulation include SEEL [19] and CASINO [20].

While such approaches are widely used, it is not rare that simulation results are substantially different from experimental results. A possible reason is that in the real system, there may be deviations from the system specifications, e.g., beam diameter, etc. Also, certain effects may not be known, or may not be easy to model. Note that experimental results reflect all phenomena/effects and actual parameters. Therefore, the motivation of this research is to develop a new method for *PSF* estimation based on experimental results, which is not constrained by a curve-fitting function and does not require a time-consuming simulation. The method is to provide an alternative or complementary approach to the conventional ones. As a first step of this research effort, feasibility of the method has been examined in this study.

The proposed method employs a single-line test pattern to estimate the forward-scattering part of *PSF*. The estimation is carried out through two steps. In the first step, the remaining resist profile of the test pattern is related to the *line spread function*, *LSF*, which is the exposure distribution when a long line is exposed. The profile is experimentally obtained and therefore realistically reflects the phenomena and parameters involved in the exposing process. The *PSF* (and therefore *LSF*) varies rapidly within the forward-scattering range. Therefore, the remaining resist profile of a single line is utilized in estimation of the forward-scattering part of *LSF*. Beyond the forward-scattering range, the *PSF* varies very slowly and its magnitude is orders of magnitude lower than in the forward-scattering range. Hence, the depth differences among lines in the multi-line profile may be utilized in estimating the backscattering part of *LSF*. In the second step, linear equations relating the *PSF* to the *LSF* are solved to obtain the *PSF* from the *LSF*. In this paper, a complete description of the proposed method for estimating the forward-scattering part is presented with the simulation and experimental results. In a future paper, the estimation of the backscattering part will be presented.

The rest of the paper is organized as follows. The relationships between the *PSF*, *LSF*, and *LRF* (*line response function*) are explained in Section 2. The two steps for estimating the forward-scattering part of *PSF*, i.e., deriving the *LSF* from the *LRF*, and the *PSF* from the *LSF*, are described in Section 3. Simulation and experimental results are presented in Section 4, followed by a summary in Section 5.

2. *PSF*, *LSF*, and *LRF*

The *LSF* is defined as the exposure distribution in the cross-section plane of resist when an infinitely long line is exposed (refer to Fig. 1). In practice, assuming a Gaussian beam, a line is written as a sequence of exposed points on a single straight path. The length of line just needs to be longer than the diameter of the electron-scattering domain. Then, the exposure distribution at the center of the line is the *LSF*. After development, the depth of the remaining resist profile in the cross-section plane is measured at each point as illustrated in Fig. 2. The depth distribution (profile) is defined as *line response function*, *LRF*. That is, the *LSF* is obtained through the convolution between the *PSF* and a long line, and the *LSF* goes through the resist development process to yield the *LRF*. The dose and developing time must be selected such that the line is not fully developed at any point, in order to extract the information on the developing rate. The relationships among the *PSF*, *LSF*, and *LRF* are depicted in Fig. 3.

One may attempt to derive a *PSF* directly from the remaining resist profile (i.e., *point response function* (*PRF*)) obtained when a single point is exposed, as illustrated in Fig. 4. However, it is extremely difficult to measure the depth profile in the cross-section passing through the exposed point, due to the tiny domain of developed region, making this approach impractical. Therefore, in this study, a two-step procedure is developed to derive the *PSF* from the *LRF* through the *LSF*. Note that it is much easier to measure the *LRF* since any cross-section away from both ends of line may be used. Also, the width of *LRF* is significantly larger than that of *PRF*, as illustrated in Fig. 4.

In a pattern of multiple features, e.g., lines, the resist profile of a feature is determined by not only its exposure but also

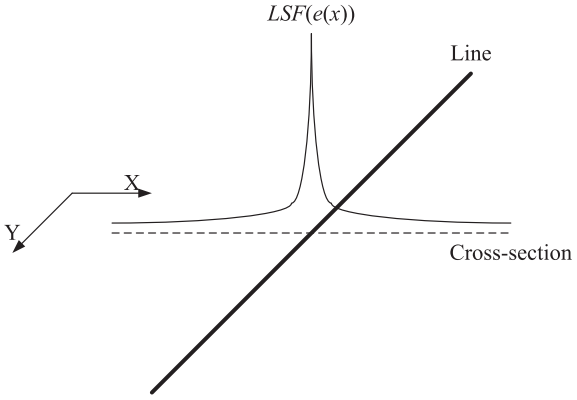

Fig. 1. Line spread function (*LSF*) which depicts the exposure distribution in the cross-section plane perpendicular to the line exposed. The line needs to be longer than twice the electron scattering range.

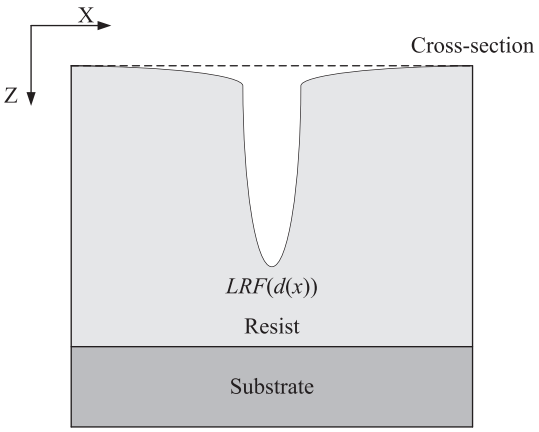

Fig. 2. Line response function (*LRF*) which is the depth distribution of remaining resist profile in the cross-section plane perpendicular to the line exposed. The line needs to be longer than twice the electron scattering range.

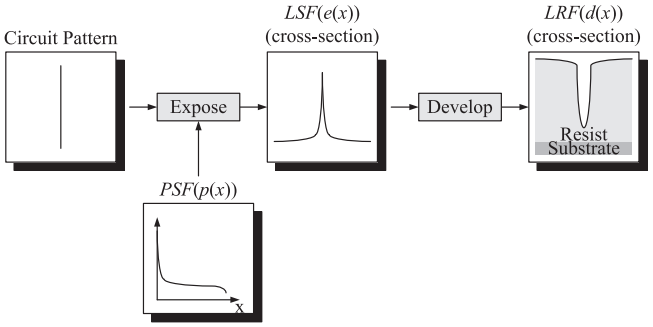

Fig. 3. Relationships among *PSF*, *LSF*, and *LRF*.

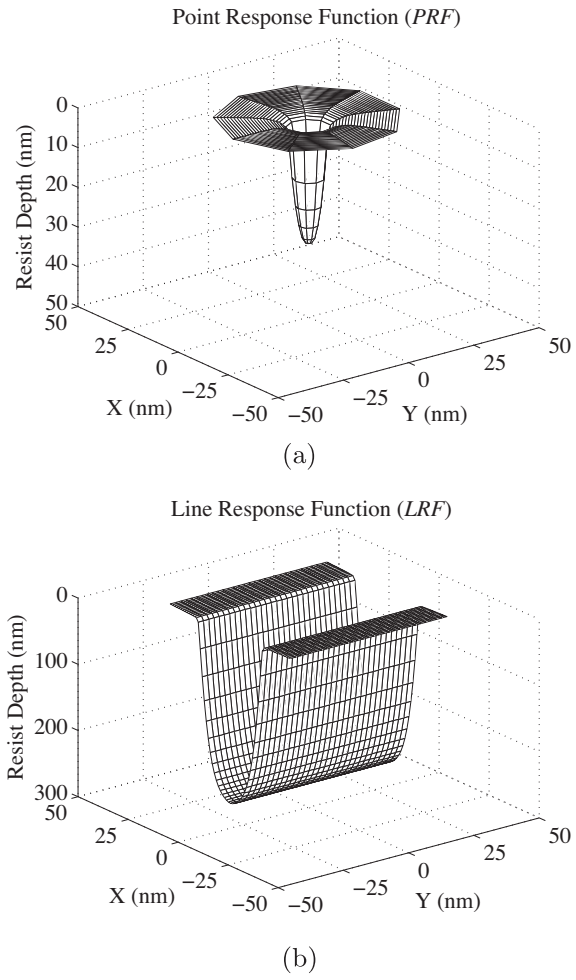

Fig. 4. Comparison of (a) point response function (*PRF*) and (b) line response function (*LRF*).

exposure contributions from other features. It would be harder to extract the forward-scattering part of *PSF* (which varies rapidly in space) from experimental results of such patterns. Hence, for estimating the forward scattering part of *PSF*, a single line is employed, which also enables exploitation of the relationship between the *LSF* and *PSF*.

3. Estimation of forward-scattering

The proposed method for estimating the forward-scattering part of *PSF* using a single-line pattern consists of two steps, from *LRF* to *LSF* and from *LSF* to *PSF*. In this paper, it is assumed that the effect of backscattering on the *LRF* is negligible since the backscattering part of *PSF* is several orders of magnitude smaller than the forward-scattering part (especially in a single-feature pattern). Nevertheless, the effect will be accounted for in the future paper which describes the estimation of the backscattering part of *PSF*.

In this study, the variation of *PSF* along the depth dimension is not considered as in most applications, i.e., 2 D *PSF*'s are estimated. The following notations are adopted for the cross-section plane:

$d(x)$: depth distribution (remaining resist profile), *LRF*
$e(x)$: exposure distribution, *LSF*
$r(x)$: developing rate distribution
$p(x)$: point spread function, *PSF*

3.1. From LRF to LSF

The *LSF* is derived from the *LRF* by first estimating the developing rate distribution from the *LRF* and then converting the rate into the exposure. Assuming that the line is oriented parallel with the *Y*-axis and sufficiently long such that any variation along the *Y*-axis can be ignored, only the cross-section of resist perpendicular to the *Y*-axis may be considered (refer to Fig. 1). Also, a 2D model is adopted, i.e., the exposure (and therefore developing rate) is averaged along the resist depth dimension. Then, the developing rate distribution in the cross-section can be expressed by a function of x only, i.e., $r(x)$. The remaining resist profile, i.e., *LRF*, is depicted by the depth profile $d(x)$. Since the resist developing process is isotropic, $d(x)$ is not linearly proportional to $r(x)$. For a given point x_i (refer to Fig. 5), $d(x_i)$ depends on not only $r(x_i)$ but also $r(x)$ in the adjacent regions. Note that x_i is a point at which *PSF* is to be estimated and does not have to be a point exposed. Though the resist is developed in all possible directions, $d(x)$ may be estimated as a combination of vertical component $d_V(x)$, i.e., the depth due to vertical development, and lateral component $d_L(x)$, i.e., the depth due to lateral development, as illustrated in Fig. 6.

The estimation of the developing rate distribution $r(x)$ is done through two phases. Let $\{x_i\}$ be the set of points at which the developing rate is to be estimated where x_0 is the point corresponding to the center of line as illustrated in Fig. 5. In the first phase, only the vertical development is taken into account. That is, the initial estimate of rate is computed as $r(x_i) = d_V(x_i)/T = d(x_i)/T$ where T is the developing time, as illustrated in Fig. 7. Then, in the second phase, $r(x)$ is iteratively adjusted to account for the lateral development, starting from the center of line. For the center point x_0, the lateral development is non-existent, thus $r(x_0)$ remains unchanged through the second phase. For the next point x_1, $d(x_1)$ includes the lateral development since $r(x_1) < r(x_0)$. And the lateral development $d_L(x_1)$ may be computed based on $r(x_0)$ and $r(x_1)$, as illustrated in Fig. 7. The depth error is computed as $\Delta d(x_1) = d_V(x_1) + d_L(x_1) - d(x_1)$, and is used to control $\Delta r(x_1)$, i.e., the increment of $r(x_1)$. Then, $d_V(x_1)$ and $d_L(x_1)$ are recomputed using the updated $r(x_1)$, generating a new $\Delta d(x_1)$. The process is repeated until $\Delta d(x_1)$ becomes less than

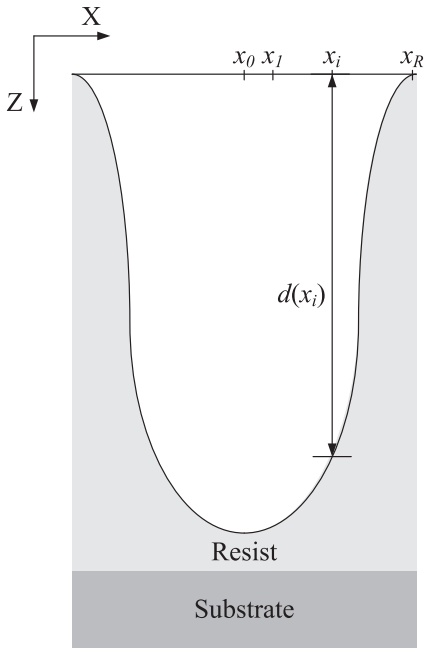

Fig. 5. Depth $d(x_i)$ at a given point x_i. Note that x_i does not have to be a point exposed.

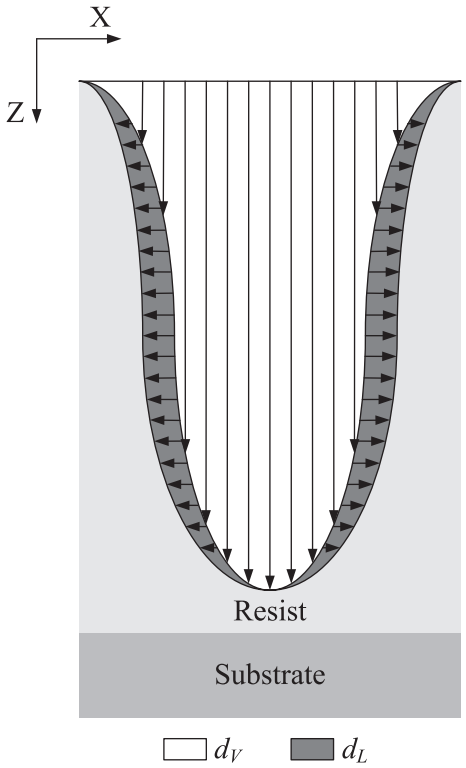

Fig. 6. The depth profile $d(x)$ may be modeled as a combination of vertical development $d_V(x)$ and lateral development $d_L(x)$.

a preset threshold. This iterative estimation recursively continues from the center of line outward for all x_i, as illustrated in Fig. 7.

From the developing rate $r(x_i)$, the exposure $e(x_i)$, i.e., *LSF*, is computed point-by-point through an exposure-to-developing-rate conversion formula which is experimentally determined. The conversion formula used in this study is given below:

$$r(x) = F[e(x)] = 4000 \cdot e^{-\left(\frac{e(x)-1.0e11}{5.8e10}\right)^2} + 50 \cdot e^{-\left(\frac{e(x)-7.0e9}{1.0e10}\right)^2} - 235 \quad (1)$$

where $r(x)$ is in nm/min and $e(x)$ in eV/μ^2.

3.2. From LSF to PSF

In general, the exposure distribution is computed by the convolution of the dose distribution of a pattern with the *PSF*. In the definition of *LSF*, the dose along a line is constant. Therefore, the exposure at a point only depends on the distance to each of the exposed points, given the constant dose. Let us consider a discrete domain as illustrated in Fig. 8. Without loss of generality, the coordinates of discrete points are assumed to be integers, i.e., $x_i = i$. The column vector e represents the set of sampled *LSF*, i.e., $(e(0), e(1), \ldots, e(R))$ where $e(0)$ is the sample at the center of *LSF* and R corresponds to the electron scattering range. Similarly, the column vector p denotes the set of sampled *PSF*, i.e., $(p(0), p(1), \ldots, p(R))$. Note that e is defined on the X-axis and the line exposed is along the Y-axis.

The exposure $e(i)$ is computed by summing up the exposure contributions from the exposed points on the line as follows:

$$\begin{aligned} e(i) &= p(i) + 2 \cdot \sum_{k=1}^{\lfloor\sqrt{R^2-i^2}\rfloor} p(\sqrt{i^2+k^2}) \\ &= p(i) + 2 \cdot \sum_{k=1}^{\lfloor\sqrt{R^2-i^2}\rfloor} ((\lfloor l \rfloor + 1 - l) \cdot p(\lfloor l \rfloor) + (l - \lfloor l \rfloor) \cdot p(\lfloor l \rfloor + 1)) \end{aligned} \quad (2)$$

where $l = \sqrt{i^2+k^2}$.

The discrete convolution to compute e can be expressed in the form of matrix multiplication:

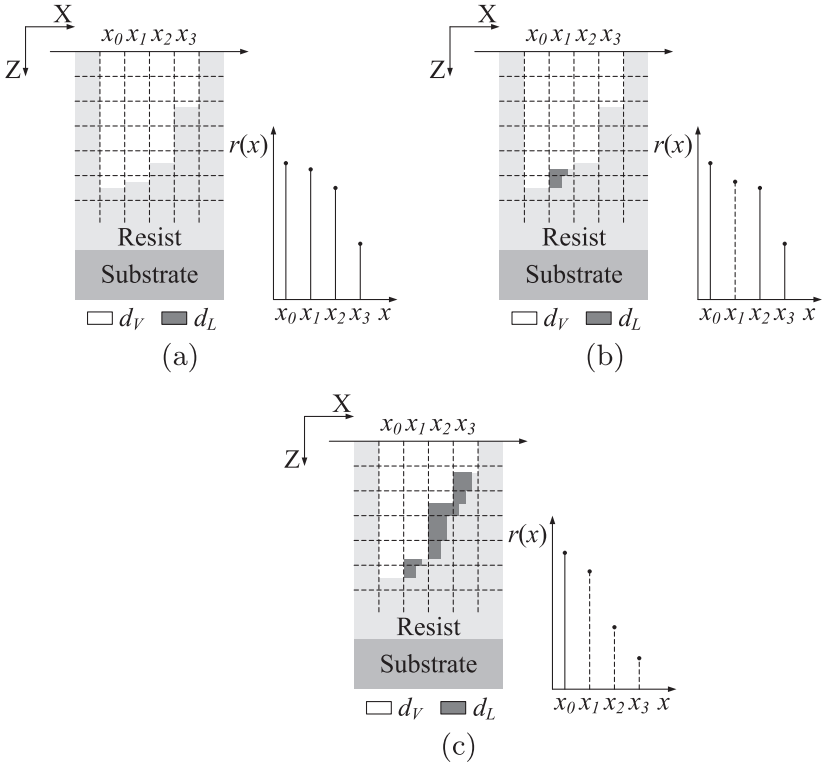

Fig. 7. Estimation of the developing rate distribution: (a) the initial $r(x_i)$, (b) after the lateral component for point x_1 is estimated, and (c) after the estimation for all points is completed.

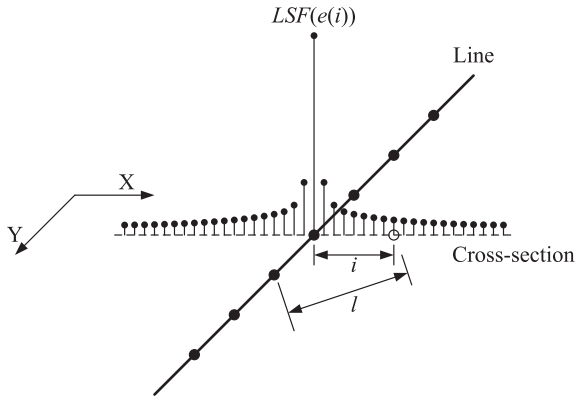

Fig. 8. The exposure at a point in the *LSF* only depends on the distances (l) to the exposed points on the line, given a uniform dose.

$$e = A \times p \tag{3}$$

where the element (i,j) of the matrix A quantifies how much $p(j)$ affects $e(i)$.

The element $A(i,j)$ can be derived by rearranging the terms in Eq. (2):

$$A(i,j) = \begin{cases} 0 & \text{for } i > j \\ 1 + 2 \cdot \sum_{k=k_2}^{k_3} (\lfloor l \rfloor + 1 - l) + 2 \cdot \sum_{k=k_1}^{k_2} (l - \lfloor l \rfloor) & \text{for } i = j \\ 2 \cdot \sum_{k=k_2}^{k_3} (\lfloor l \rfloor + 1 - l) + 2 \cdot \sum_{k=k_1}^{k_2} (l - \lfloor l \rfloor) & \text{for } i < j \end{cases} \tag{4}$$

where $k_1 = \lceil \sqrt{(j-1)^2 - i^2} \rceil$, $k_2 = \lceil \sqrt{j^2 - i^2} \rceil$ and $k_3 = \lfloor \sqrt{(j+1)^2 - i^2} \rfloor$.

As long as the sizes of the vectors p and e are the same, the square matrix A is invertible since A is an upper triangular matrix. Then, the *PSF* can be computed by

$$p = A^{-1} \times e \tag{5}$$

The computational requirement in this step can be significant depending on the sampling interval since the size of A can be very large. However, this problem can be easily alleviated by employing non-uniform sampling in order to exploit the fact that the *PSF* varies fast only for a short range beyond which it changes very slowly. In the short range, the *PSF* is sampled sufficiently finely, but the sampling interval is increased progressively.

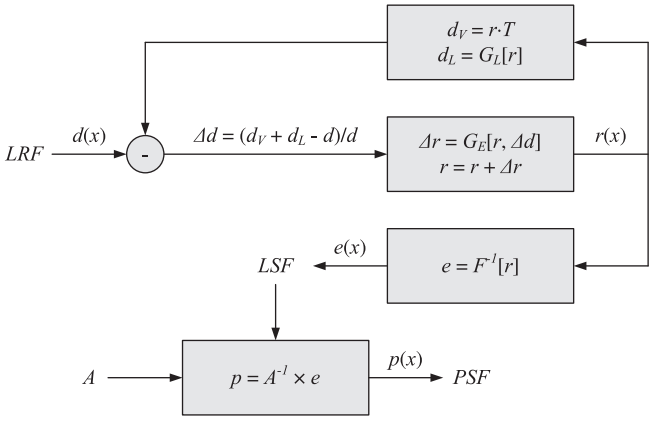

Fig. 9. Flowchart of the proposed estimation scheme.

3.3. Procedure

The procedures for estimating the forward-scattering part of *PSF*'s are summarized below and also depicted in Fig. 9.

Step 0: The developing rate at the center point x_0 is computed as $r(x_0) = d(x_0)/T$ where T is the developing time and set i to 1.

Step 1: At the point x_i, compute the initial developing rate distribution from a depth profile $d(x_i)$, i.e., *LRF*. That is, $r(x_i) = d(x_i)/T$.

Step 2: Compute the vertical development $d_V(x_i) = r(x_i) \cdot T$ and lateral development $d_L(x_i) = G_L[r(x_k)|k = 0,1,2,\ldots,i]$, where $G_L[\cdot]$ given in Eq. (6) represents the process of estimating the lateral development

$$\begin{aligned} d_L(x_i) &= G_L[r(x_k) \,|\, k = 0,1,2,\ldots,i] \\ &= \sum_{j=1}^{i} \int_{r(x_j)\cdot T}^{r(x_{j-1})\cdot T} r(x_i) \cdot \left(T - \frac{z}{r(x_{j-1})} - \sum_{k=j}^{i-1} \frac{W_P}{r(x_k)} \right) \cdot \frac{dz}{(r(x_{j-1}) - r(x_j)) \cdot T} \end{aligned} \tag{6}$$

where $r(x_i) \cdot \left(T - \frac{z}{r(x_{j-1})} - \sum_{k=j}^{i-1} \frac{W_P}{r(x_k)} \right)$ is limited between 0 and W_p, and $W_p = x_i - x_{i-1}$.

Step 3: If the percentage depth error $\Delta|d(x_i)| = |(d_V(x_i) + d_L(x_i) - d(x_i))/d(x_i)|$ is smaller than a certain threshold, go to Step 4. Otherwise, compute $\Delta r(x_i) = G_E[r, \Delta d(x_i)]$ where $G_E[\cdot]$ given in Eq. (7) is a function used for controlling the increment/decrement of $r(x_i)$, update $r(x_i) = r(x_i) + \Delta r(x_i)$, and go back to Step 2.

$$\begin{aligned} \Delta r(x_i) &= G_E[r(x_i), \Delta d(x_i)] \\ &= r(x_i) \cdot (-sgn(\Delta d(x_i)) \cdot \alpha) \end{aligned} \tag{7}$$

where α is a preset constant between 0 and 1.

Step 4: If the developing rates at all points have been estimated, go to Step 5. Otherwise, $i = i + 1$ and go back to Step 1.

Step 5: Compute the exposure distribution, i.e., *LSF*, by $e(x_i) = F^{-1}[r(x_i)]$, where $F[\cdot]$ is the exposure-to-developing-rate conversion formula given by Eq. (1).

Step 6: For each point at which the *LSF* is examined, calculate its distance from each exposed point (refer to Fig. 8). Based on the distances, generate matrix A according to Eq. (4).

Step 7: Derive the *PSF* from the *LSF* by $p = A^{-1} \times e$ which can be effectively considered as a deconvolution process.

4. Results and discussion

The proposed estimation method has been tested first through simulation where *PSF*'s generated by a Monte Carlo method (SEEL [19]) are employed, in order to examine its feasibility. From a *PSF*, the *LSF* is computed by the convolution, the *LRF* is obtained through the developing rate conversion and development

Table 1
Difference between the estimated *PSF* and Monte Carlo simulated *PSF*.

PSF		Difference	
PMMA thickness (nm)	Beam energy (keV)	Mean percentage difference (%)	Max percentage difference (%)
100	5	3.92	9.29
	20	2.33	6.83
	50	5.85	15.47
300	5	5.92	13.30
	20	1.71	5.63
	50	2.64	7.25
500	5	4.84	14.89
	20	6.65	13.99
	50	4.59	7.69

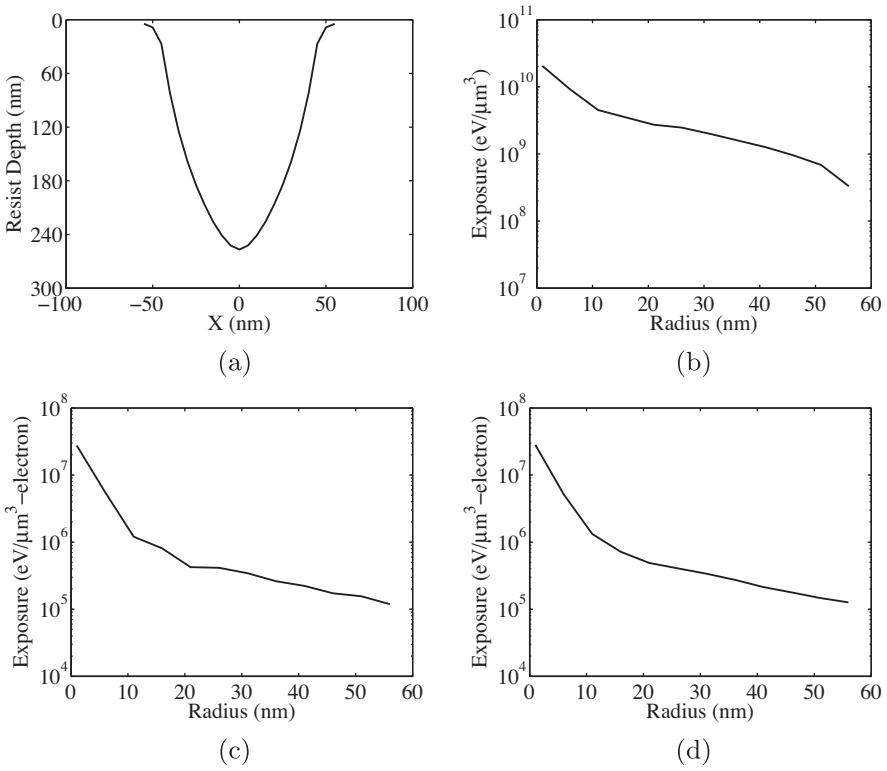

Fig. 10. Simulation results (300 nm PMMA on Si and 5 keV): (a) *LRF* generated from Monte Carlo simulated *PSF*; (b) *LSF* estimated from *LRF*; (c) *PSF* estimated from *LSF*; (d) *PSF* generated by Monte Carlo simulation.

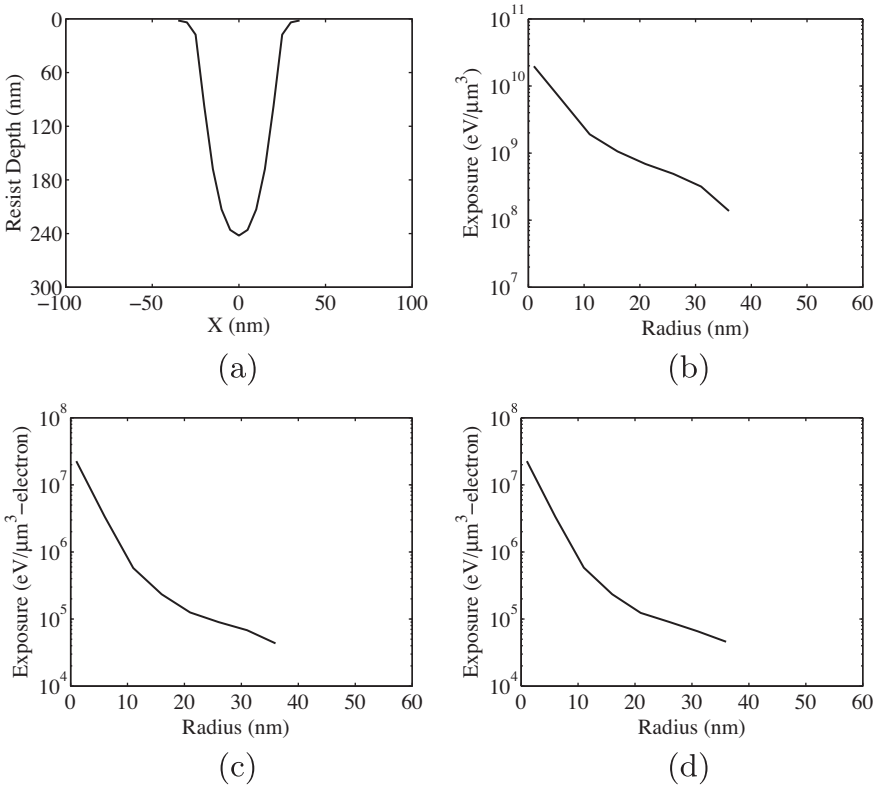

Fig. 11. Simulation results (300 nm PMMA on Si and 20 keV): (a) *LRF* generated from Monte Carlo simulated *PSF*; (b) *LSF* estimated from *LRF*; (c) *PSF* estimated from *LSF*; (d) *PSF* generated by Monte Carlo simulation.

simulation, and then the proposed estimation scheme is employed to estimate the *PSF* from the *LRF*. The estimated *PSF* is compared back to the original *PSF*. Note that the purpose of this simulation study is to verify the accuracy of the proposed method, i.e., if it

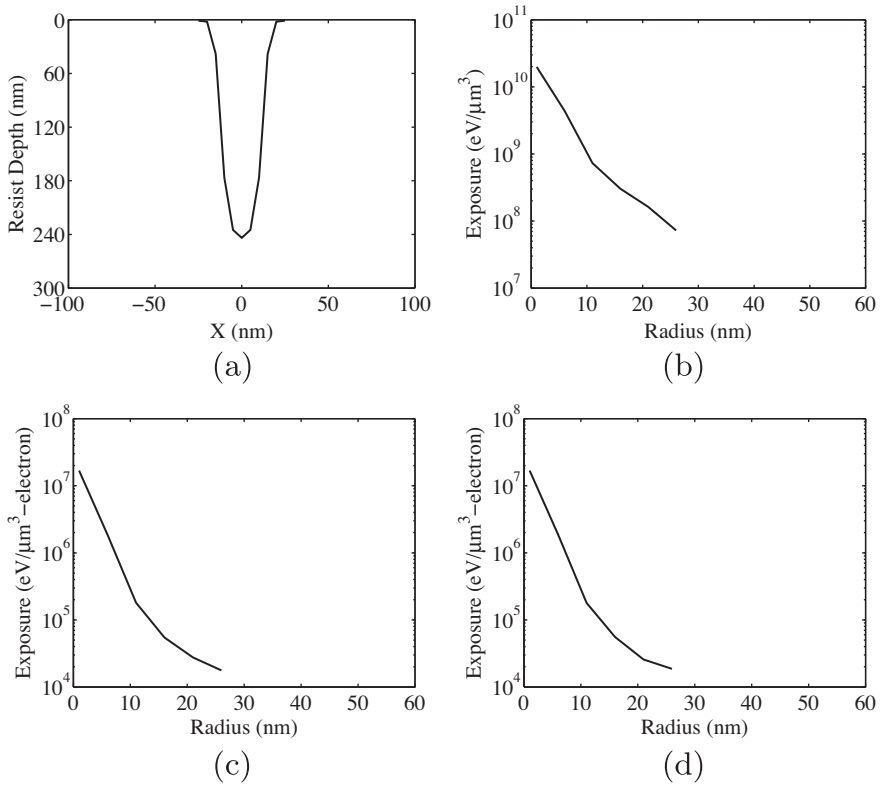

Fig. 12. Simulation results (300 nm PMMA on Si and 50 keV): (a) *LRF* generated from Monte Carlo simulated *PSF*; (b) *LSF* estimated from *LRF*; (c) *PSF* estimated from *LSF*; (d) *PSF* generated by Monte Carlo simulation.

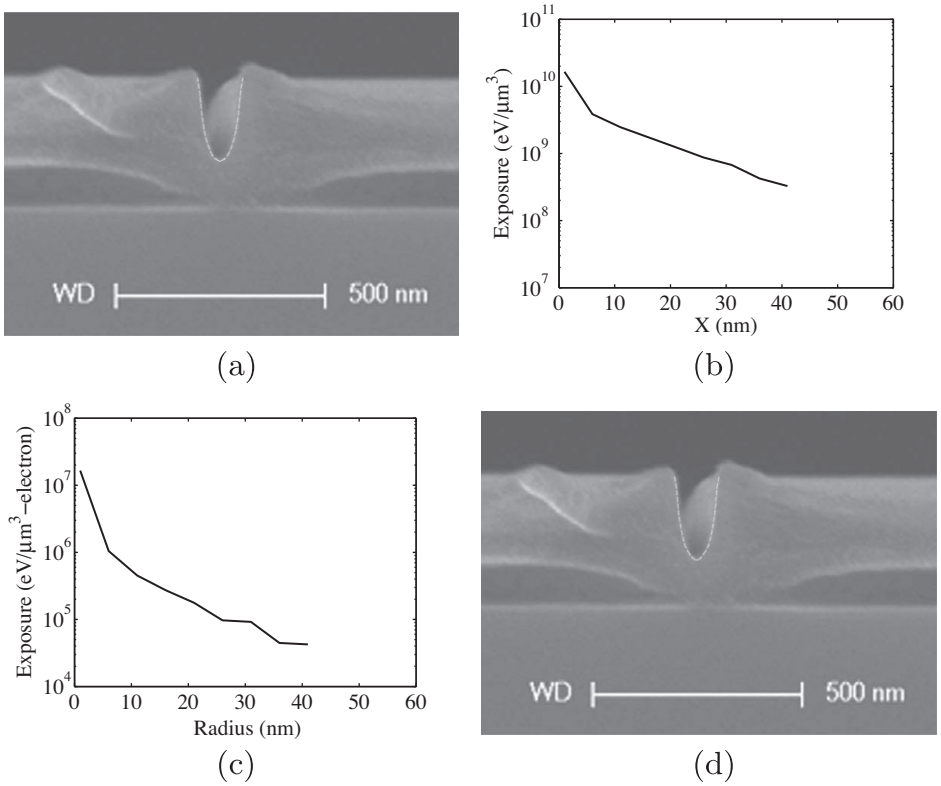

Fig. 13. Experimental results (300 nm PMMA on Si and 50 keV): (a) *LRF* measured from the SEM image of resist profile; (b) *LSF* estimated from *LRF*; (c) *PSF* estimated from *LSF*; (d) *LRF* reconstructed from the estimated *PSF* through simulation.

is able to derive the original PSF from the LRF generated through the simulated experimental process. The substrate systems employed in the simulation are composed of PMMA on Si where the three different PMMA thicknesses, 100, 300, and 500 nm, are

considered for each of the three different beam energies 5, 20, and 50 keV. These nine combinations should cover a broad set of different shapes of *PSF*'s. Note that as the beam energy is increased, the forward-scattering range is reduced and the backscattering range is increased [21].

The performance of the proposed estimation method is evaluated in terms of the mean and maximum percentage differences, which are defined as:

$$\textit{Mean percentage difference} = \frac{1}{n}\sum_{i=1}^{n}\frac{|\,PSF'_i - PSF_i\,|}{PSF_i}\times 100\% \tag{8}$$

$$\textit{Max percentage difference} = \max_{i=1}^{n}\frac{|\,PSF'_i - PSF_i\,|}{PSF_i}\times 100\% \tag{9}$$

where PSF'_i is the ith value of the estimated *PSF*, PSF_i is the ith value of the original *PSF* generated by the Monte Carlo simulation [19], and n is the number of samples in each of the *PSF* and *PSF*′.

It can be observed in Table 1 that the mean percentage differences are very small, i.e., in the range of 1.71–6.65%. The results for 300 nm PMMA with 5, 20, and 50 keV are plotted in Figs. 10–12, respectively, where it is seen that the estimated *PSF*'s match very well with the original *PSF*'s.

The proposed estimation method has been tested also via experiment. A Si wafer was spin-coated with 300 nm PMMA and soft-baked at 160 °C for 1 min. A long line was exposed with a high dose (2500 μC/cm^2) using ELIONIX ELS-7000 e-beam lithography system (50 keV) and the sample was developed in MIBK:IPA = 1:2 for 40 s. The high dose is to obtain a significant developed depth while exposing a line. The *LRF* was measured from the cross-section SEM image of resist profile (the yellow curve in Fig. 13).[1] The *LSF* (Fig. 13) was estimated from the *LRF* and then the *PSF* (Fig. 13) from the *LSF*. In order to examine the accuracy of the estimated *PSF*, the *LRF* (the yellow curve in Fig. 13) was reconstructed through simulation using the estimated *PSF*. The mean percentage error between the measured and reconstructed *LRF*'s (remaining resist profiles) is 7.35%, demonstrating high accuracy of the proposed estimation method.

5. Summary

An experiment-based approach to estimating the forward-scattering parts of *PSF*'s is proposed to provide an alternative to the conventional approaches. The proposed method utilizes the resist profile of a single line for the estimation of a *PSF* in the forward-scattering range. From the resist profile, the *LSF* is derived and then the *PSF* is computed by solving a set of linear equations formulated based on the mathematical relationship between the *LSF* and *PSF*. The feasibility of the proposed approach has been examined through simulation and also experiments. The results indicate that the proposed approach has a good potential to enable a new *PSF*-estimation method complementary to the existing ones. The *PSF*'s obtained by the proposed method which utilizes data from experiments are likely to produce simulation results consistent with experimental results. The current research includes development of the estimation method for the backscattering part of *PSF*.

Acknowledgements

This work was supported by a research grant from Samsung Electronics Co., Ltd. The authors thank National NanoFab Center for experiment and characterization services.

References

[1] R. Rau, J. McClellan, T. Drabik, J. Vac. Sci. Technol. B 14 (4) (1996).
[2] S.-Y. Lee, B.D. Cook, IEEE Trans. Semicond. Manuf. 11 (1998) 108.
[3] C.S. Ea, A.D. Brown, J. Vac. Sci. Technol. B 17 (2) (1999).
[4] K. Takahashi, M. Osawa, M. Sato, H. Arimoto, K. Ogino, H. Hoshino, Y. Machida, J. Vac. Sci. Technol. B 18 (6) (2000).
[5] M. Osawa, K. Takahashi, M. Sato, H. Arimoto, K. Ogino, H. Hoshino, Y. Machida, J. Vac. Sci. Technol. B 19 (6) (2001).
[6] S.-Y. Lee, K. Anbimony, J. Vac. Sci. Technol. B 25 (6) (2006).
[7] A. Moniwa, H. Yamaguchi, S. Okazaki, J. Vac. Sci. Technol. B 10 (6) (1992).
[8] S.-Y. Lee, K. Anbumony, J. Vac. Sci. Technol. B 25 (6) (2007).
[9] S.-Y. Lee, S.C. Jeon, J.S. Kim, K.N. Kim, M.S. Hyun, J.J. Yoo, J.W. Kim, J. Vac. Sci. Technol. B 27 (6) (2009).
[10] P. Li, S.-Y. Lee, S.C. Jeon, J.S. Kim, K.N. Kim, M.S. Hyun, J.J. Yoo, J.W. Kim, J. Vac. Sci. Technol. B 28 (1) (2010).
[11] T.H.P. Chang, J. Vac. Sci. Technol. 12 (6) (1975).
[12] S.J. Wind, M.G. Rosenfield, G. Pepper, W.W. Molzen, P.D. Gerber, J. Vac. Sci. Technol. B 7 (6) (1989).
[13] M. Gentili, L. Grella, A. Lucchesini, L. Luciani, L. Mastrogiacomo, P. Musumeci, J. Vac. Sci. Technol. B 8 (6) (1990).
[14] K.-S. Yu, J.-C. Lee, J. Korean Phys. Soc. 28 (4) (1995).
[15] S.A. Rishton, D.P. Kern, J. Vac. Sci. Technol. B 5 (1) (1987).
[16] R.H. Fastenau, K.M. Monahan, D.F. Kyser, S. Phelps, J. Vac. Sci. Technol. B 7 (6) (1989).
[17] T.A. Fretwell, R. Gurung, P.L. Jones, Microelectron. Eng. 17 (1–4) (1992).
[18] M. Rooks, N. Belic, E. Kratschmer, R. Viswanathan, J. Vac. Sci. Technol. B 23 (6) (2005).
[19] S. Johnson, Ph.D. Dissertation, Simulation of Electron Scattering in Complex Nanostructures: Lithography, Metrology, and Characterization, Cornell University Ithaca, NY, 1992.
[20] D. Drouin, A.R. Couture, D. Joly, X. Tastet, V. Aimez, R. Gauvin, Scanning 29 (3) (2007).
[21] E. Anderson, D. Olynick, W. Chao, B. Harteneck, E. Veklerov, J. Vac. Sci. Technol. B 19 (6) (2001).

[1] For interpretation of color in Fig. 13, the reader is referred to the web version of this article.